# Characterization method for relative Raman enhancement for surface-enhanced Raman spectroscopy using gold nanoparticle dimer array

Sugano, Koji

Ikegami, Kohei

Isono, Yoshitada

1 **Characterization method for relative Raman enhancement**

2 **for surface-enhanced Raman spectroscopy using gold**

3 **nanoparticle dimer array**

4 Koji Sugano*, Kohei Ikegami, and Yoshitada Isono

5 *Department of Mechanical Engineering, Graduate School of Engineering, Kobe University,*

6 *Kobe 657-8501, Japan*

7 *E-mail: sugano@mech.kobe-u.ac.jp

8

9 In this paper, a characterization method for Raman enhancement for highly sensitive and

10 quantitative surface-enhanced Raman spectroscopy (SERS) is reported. A particle dimer

11 shows a marked electromagnetic enhancement when the particle connection direction is

12 matched to the polarization direction of incident light. In this study, dimers were arrayed by

13 nanotrench-guided self-assembly for a marked total Raman enhancement. By measuring

14 acetonedicarboxylic acid, the fabricated structures were characterized for SERS depending

15 on the polarization angle against the particle connection direction. This indicates that the

16 fabricated structures cause an effective SERS enhancement, which is dominated by the

17 electromagnetic enhancement. Then, we measured 4,4'-bipyridine, which is a pesticide

18 material, for quantitative analysis. In advance, we evaluated the enhancement of the particle

19 structure by the Raman measurement of acetonedicarboxylic acid. Finally, we compared the

20 Raman intensities of acetonedicarboxylic acid and 4,4'-bipyridine. Their intensities showed

21 good correlation. The advantage of this method for previously evaluating the enhancement

22 of the substrate was demonstrated. This developed SERS characterization method is

23 expected to be applied to various quantitative trace analyses of molecules with high

24 sensitivity.

25

## 1. Introduction

Surface-enhanced Raman spectroscopy (SERS) is a powerful tool for bio/chemical trace analysis because of its high sensitivity and high molecular identification ability without labeling.[1-4] A Raman spectrum includes molecular structural information showing several Raman peaks corresponding to a molecular structure. Therefore, it has been expected to be applied to various fields such as medicine, biology, and environment.[2,5-8] The Raman scattering light from a small number of molecules is significantly weak. In SERS, however, the Raman scattering light can be enhanced by plasmonic resonance, which occurs on metal nanostructure surfaces.[2,3] Therefore, SERS enables us to perform the highly sensitive rapid detection and reliable identification of bio/chemical molecules.

For SERS, various enhancing nanostructures such as those obtained by particle aggregation,[7,9] carbon nanotube (CNT) aggregation,[10] and nanoporous fabrication[11] have been reported. These nanostructures consist of numerous nanogaps called hotspots. A strategy of these method is to fabricate numerous nanogaps. However, it has been known that Raman enhancement shows a polarization-dependent property of an incident light. Many theoretical studies have supported this polarization dependent Raman enhancement.[4,12] Single-molecule SERS detection has been performed using a gold nanoparticle dimer with a molecular bridge between particles when the polarization direction of an incident light is matched to the particle-particle connection direction.[13,14] However, the connecting direction cannot be controlled on a substrate for on-substrate SERS measurement.[12,14] Moreover, it is necessary to adjust the polarization direction to the connecting direction of particles for each dimer after scanning electron microscopy (SEM) or atomic force microscopy (AFM) observation. Therefore, this method is inefficient for the practical applications of SERS. In addition to the above problems, Raman intensities showed a large variation in the reported SERS experiments. Raman intensity variation has been thought to originate from the distributions of particle arrangement characteristics such as nanogap, particle morphology, the number of hotspots, particle configuration, and particle connecting direction.

To overcome these problems, therefore, we proposed the use of a directionally and regularly arrayed gold nanoparticle dimer as shown in Fig .1. In this structure, two gold nanoparticles configure a particle dimer and dimers are arranged directionally and

57  regularly on a substrate. Therefore, it is unnecessary to adjust the polarization direction of

58  an incident light for each dimer. A particle dimer is fabricated by drying-based nanotrench-

59  guided self-assembly.[15-19] Particle surfaces are covered by citrate, acetonedicarboxylic acid,

60  acetoacetic acid, and intermediate products after chemical synthesis using a citrate reduction

61  method.[20-22] During the drying process in the self-assembly, the adsorbed molecule layer

62  acts as a spacer between particles, forming a nanogap between particles. The thickness of

63  the citrate groups is around 0.5 nm.[23] Therefore, a nanogap of around 1 nm forms between

64  particles. Before the SERS analysis for target molecules in the solution, the adsorbed

65  molecules were removed. Although electron beam (EB) lithography or focused ion beam

66  (FIB) has been used for fabricating orderly nanostructures,[15-19] one cannot fabricate a

67  nanogap of around 1 nm, which shows a marked electromagnetic enhancement.[24,25] We

68  confirmed that the proposed structures enable us to perform an ultrasensitive and rapid SERS

69  analysis.[19,26]

70      In our structures, however, the obtained Raman intensities showed large variations as

71  with the previously reported SERS substrates. The distributions of the number of hotspots,

72  particle configuration, and particle connecting direction, mentioned above as reasons for

73  large variations in Raman intensities, should be smaller in our substrate. The Raman intensity

74  variation from our substrate is thought to be due to the distributions of nanogap and particle

75  morphology in the subnanometer scale. The nanogap has a significant effect on Raman

76  enhancement.[27] These features are difficult to be controlled.

77      Therefore, we propose a characterization method for a relative Raman enhancement in

78  this study. A gold nanoparticle chemically synthesized by a citrate reduction method has

79  adsorbed molecules on particle surfaces. We used the adsorbed molecules for preliminary

80  characterization. Although the adsorbed molecules are removed before the SERS analysis

81  for target molecules, Raman intensities from the adsorbed molecules are preliminarily

82  measured for each dimer array. Then, target molecules, 4,4'-bipyridine in this study, are

83  measured after removing the adsorbed molecules. On the basis of the SERS intensities from

84  the adsorbed molecules, we can choose the SERS substrate that shows a higher Raman

85  enhancement. Furthermore, the Raman intensities obtained from target molecules can be

86  compensated using the Raman intensities from the adsorbed molecules. In this study, we

87  evaluated the proposed method by investigating the (1) polarization angle dependence and

88    (2) Raman intensity relationship between the adsorbed and 4,4'-bipyridine molecules.

89

## 2. Experimental and analytical methods

91    2.1 SERS structure and fabrication process

92    The directionally and regularly arrayed gold nanoparticle dimers are shown in Fig. 1. In this

93    study, gold nanoparticles with a mean particle diameter of approximately 100 nm were used.

94    The nanoparticles were arranged along the template nanotrenches on a Si substrate using a

95    nanotrench-guided self-assembly method.[16-20] The connection direction of the arranged

96    nanoparticles was easily matched to the polarization direction of the incident light without

97    SEM or AFM observation. The intervals of the arranged dimers were 400 and 200 nm in the

98    directions parallel and perpendicular to the coupling direction of the particles, respectively.

99        The nanotrench-guided self-assembly used in this study is shown in Fig. 2. A colloidal

100   particle solution was injected between a cover glass and a template substrate with an array

101   of nanotrenches. The Si template substrate was etched by inductively coupled plasma

102   reactive ion etching (ICP-RIE) with an EB resist mask pattern. The water surface line moved

103   backward and the particles became concentrated near the meniscus edge during the drying

104   of the aqueous particle dispersion between the substrates. The drag force pressed the

105   particles onto the template substrate to trap the particles on the template nanotrenches when

106   the meniscus passed over the templates. The gold nanoparticles were synthesized by a citrate

107   reduction method. The synthesized particles exhibited negatively charged surfaces because

108   acetonedicarboxylic acid, acetoacetic acid, and citrate molecules uniformly formed and

109   attached to the particle surfaces without vacancy during synthesis.[23] During the removal of

110   the remaining water between the particles, the particles attract each other and form particle–

111   particle contacts, which act as hotspots. A nanogap of around 1 nm forms between particles.

112   2.2 Characterization method for relative Raman enhancement

113   Raman measurements were performed using a micro-Raman spectroscopy system equipped

114   with a He-Ne laser of 632.8 nm wavelength. A ×50 objective lens with an NA of 0.5 was

115   used. The laser spot size was approximately 2 μm. For all measurements, mapping Raman

116   measurements were carried out in a $7 \times 7$ μm$^2$ area with an interval of 1 μm. The center of the

117   mapping area was located at the arrangement area of dimers of $5 \times 5$ μm$^2$. The integration

118 time was set to 2 s. The Raman intensities integrated from 1500 to 1700 cm$^{-1}$ were used for

119 characterization because the maximum intensity was observed in that Raman spectra range.

120 As the first experiment, we investigated the dependence of Raman intensities on the

121 polarization angle of an incident light. In this experiment, the molecules adsorbed on the

122 particle surfaces were used for characterization. After arranging the particles, pure water was

123 placed in a poly(dimethylsiloxane) (PDMS) reservoir, as shown in Fig. 1, and then Raman

124 measurements were carried out. The substrate direction was adjusted through the

125 microscopic observation of the square arrangement area. The polarization angle in the

126 coupling direction was varied from 0 to 90° in 15° increments. The adjustment accuracy was

127 approximately ±1°. Then, the dependence was compared with the simulation result of the

128 Raman enhancement factor. The Raman enhancement factor $|E|^4$ at the wavelength of an

129 incident light was calculated from the simulated electromagnetic enhancement factor $|E|^2$ at

130 a nanogap.[12,28-32] It was simulated by a commercially available finite differential time

131 domain (FDTD) software program. The nanogap between particles was set to 1 nm in this

132 simulation.

133 Next, we compared the Raman intensities of the adsorbed and 4,4'-bipyridine molecules

134 for the same dimer array. First, we obtained the Raman spectrum of the adsorbed molecules

135 at a polarization angle of 0°. Then, we acquired the Raman spectrum of the 4,4'-bipyridine

136 molecules after removing the adsorbed molecules by UV/O$_3$ treatment at 80 °C and 40 min.

137 We confirmed from the Raman spectrum that the adsorbed molecules were completely

138 removed. $10^{-3}$ and $10^{-7}$ M 4,4'-bipyridine solutions were prepared by dissolving a powder

139 in pure water. The prepared solution was placed in a PDMS reservoir as shown in Fig. 1.

140

## 3. Results and discussion

### 3.1 Fabrication

143 Figure 3 shows the SEM images of the arrangement of the fabricated gold nanoparticles. We

144 observed that gold nanoparticles were arranged onto the nanotrench template and gold

145 nanoparticle dimers were arrayed directionally and regularly. Although the length of the

146 nanotrench was 260 nm, two particles with a mean dimeter of 100 nm were connected by

147 water bridge force during the drying process. All the connection directions of particles were

148 in one direction. In the arranged particles, we found the distributions of particle size, shape,

149 and the number of hotspots. These distributions are one of the reasons for the observed

150 Raman intensity variations.

## 3.2 Raman spectroscopy: polarization-dependent property

152 Figure 4 shows the Raman spectra acquired from the adsorbed molecules on particles

153 surfaces. We observed large broad peaks at Raman shifts from 1000 to 1400 $cm^{-1}$ and from

154 1500 to 1700 $cm^{-1}$. These peaks were thought to originate from the adsorbed molecules.

155 These peaks disappeared after the UV/$O_3$ treatment. The broad peak at around 950 $cm^{-1}$

156 originated from the Si substrate. The Raman intensity increased with decreasing polarization

157 angle as shown in Fig. 4.

158 Figure 5 shows the mapping result with the interval of 1 μm. In this result, higher Raman

159 intensities were observed in the 5×5 $\mu m^2$ region, which is the arrangement area. We

160 confirmed that the gold nanoparticle array exhibits a strong enhancement. Figure 6 shows

161 the polarization angle dependences of the normalized experimental Raman intensity and

162 simulated Raman enhancement. These dependences showed good agreement between the

163 experimental and simulation results. The small difference observed at a polarization angle

164 between 15° and 60° is thought to be due to a chemical enhancement effect caused by charge

165 transfer and/or the orientation of molecules adsorbed on particle surfaces. These results

166 indicate that all dimers were arranged in one direction on a substrate and an effective Raman

167 enhancement was possible. Furthermore, Raman intensities were dominated by the

168 electromagnetic enhancement. Therefore, the proposed method using the adsorbed

169 molecules was suitable for the characterization of relative Raman enhancement.

## 3.3 Raman spectroscopy: 4,4'-bipyridine detection

171 Figures 7 and 8 show the typical Raman spectra obtained from the adsorbed molecules and

172 4,4'-bipyridine solution, respectively. The letters in Figs. 7 and 8 indicate the sample

173 numbers. Lines A–C and D–F in Fig. 8 show the Raman spectra obtained from $10^{-3}$ and $10^{-7}$

174 M solutions, respectively, using different substrates. In Fig. 8, several Raman peaks, which

175 originate from 4,4'-bipyridine,[33] are shown as dotted lines. In both cases in Figs. 7 and 8,

176 Raman intensities exhibit large variations.

177 Figure 9 shows the relationship between the Raman intensities of the adsorbed and 4,4'-

178 bipyridine molecules at $10^{-3}$ and $10^{-7}$ M. The letters in Fig. 9 indicate the sample numbers

179 shown in Figs. 7 and 8. They show a linear correlation between the Raman intensities. We

180    confirmed that the Raman intensities are affected by the SERS structure. The dotted lines

181    indicate the linearly fitted lines. The slopes were 0.123 and 0.062 for $10^{-3}$ and $10^{-7}$ M,

182    respectively.

183        Then, we proposed a compensation method for reducing Raman intensity variations from

184    4,4'-bipyridine using the obtained correlation slope $s$. The compensated intensity of 4,4'-

185    bipyridine $I'^{P}_{i}$ was calculated from $I'^{P}_{i} = I^{P}_{i} + (2000 - I^{A}_{i}) \times s$. Here, $I^{A}_{i}$ and $I^{P}_{i}$

186    indicate the Raman intensities from the adsorbed and target molecules, respectively. 2000

187    indicates the standard intensity of the adsorbed molecules, which was determined to be

188    comparable to the average of the adsorbed molecules in this study. This means that the

189    Raman intensity of 4,4'-bipyridine calculated using the obtained slope of the fitting line when

190    the preliminary Raman intensity of the adsorbed molecules is 2000 counts. Figure 10 shows

191    the set of Raman intensities of 4,4'-bipyridine depending on its concentration before and

192    after the compensation shown in Fig. 9. Table I shows a summary of the average, standard

193    deviation, and coefficient value (CV) of Raman intensities. The average intensity at $10^{-3}$ M

194    was only 1.7 times higher than that of $10^{-7}$ M. We considered that this is due to the fact that

195    the number of molecules generating the Raman scattering light is not proportional to the

196    molecular concentration owing to the limited number of hotspots and area. The CV values

197    of 4,4'-bipyridine after compensation at $10^{-3}$ and $10^{-7}$ M were 10.9 and 11.4%, respectively.

198    The CV was significantly reduced by compensation. The proposed characterization method

199    enables us to choose a highly enhancing SERS substrate and reduce the variation in Raman

200    intensity.

201

## 4. Conclusions

202

203    In this study, we proposed a characterization method for reducing the variation in Raman

204    intensity for a directionally arrayed gold nanoparticle dimer. The SERS structure was

205    fabricated by nanotrench-guided self-assembly. All particles were connected in one direction.

206        We confirmed from the polarization dependence that Raman intensities are dominated

207    by the electromagnetic enhancement and that the proposed method using the adsorbed

208    molecules is suitable for the characterization of relative Raman enhancement. These results

209    show a linear correlation between the Raman intensities. We confirmed that the Raman

210    intensities are mainly affected by the SERS structure. The proposed characterization method

211    enables us to choose a highly enhancing SERS substrate. The CV values of 4,4'-bipyridine

212    after compensation at $10^{-3}$ and $10^{-7}$ M were 10.9 and 11.4%, respectively, and CV was

213    significantly reduced by compensation.

214

## Acknowledgments

223

## References

1) K. Kneipp, H. Kneipp, I. Itzkan, R. R. Dasari, and M. S. Feld, Chem. Rev. **99**, 2957 (1999).

2) D. Cialla, A. März, R. Böhme, F. Theil, K. Weber, M. Schmitt, and J. Popp, Anal. Bioanal. Chem. **403**, 27 (2012).

3) S-C. Luo, K. Sivashanmugan, J-D. Liao, C-K. Yao, and H-C. Peng, Biosens. Bioelectron. **61**, 232 (2014).

4) H. Xu, J. Aizpurua, M. Käll, and P. Apell, Phys. Rev. E **62**, 4318 (2000).

5) K. Kneipp, H. Kneipp, I. Itzkan, R. R. Dasari, and M. S. Feld, Curr. Sci. **77**, 915 (1999).

6) C. Otto, T. J. J. van den Tweel, F. F. M. de Mul, and J. Greve, J. Raman Spectrosc. **17**, 289 (1986).

7) P. C. Pinheiro, S. Fateixa, H. I. S. Nogueira, and T. Trindade, J. Raman Spectrosc. **46**, 47 (2015).

8) S. E. J. Bell and N. M. S. Sirimuthu, J. Am. Chem. Soc. **128**, 15580 (2006).

9) R. G. Freeman, K. C. Grabar, K. J. Allison, R. M. Bright, J. A. Davis, A. P. Guthrie, M. B. Hommer, M. A. Jackson, P. C. Smith, D. G. Walter, and M. J. Natan, Science **267**, 1629 (1995).

10) A. O. Altun, S. K. Youn, N. Yazdani, T. Bond, and H. G. Park, Adv. Mater. **25**, 4431 (2013).

11) H. Liu, L. Zhang, X. Lang, Y. Yamaguchi, H. Iwasaki, Y. Inouye, Q. Xue, and M. Chen, Sci. Rep. **1**, 112 (2011).

12) K. Yoshida, T. Itoh, H. Tamaru, V. Biju, M. Ishikawa, and Y. Ozaki, Phys. Rev. B **81**, 115406 (2010).

13) K. Kneipp, H. Kneipp, V. B. Kartha, R. Manoharan, G. Deinum, I. Itzkan, R. R. Dasari, and M. S. Feld, Phys. Rev. E **57**, R6281 (1998).

14) S. Nie, and S. Emory, Science **275**, 1102 (1997).

15) K. Sugano, T. Ozaki, T. Tsuchiya, and O. Tabata, Sens. Mater. **23**, 263 (2011).

16) T. Ozaki, K. Sugano, T. Tsuchiya, and O. Tabata, J. Microelectromech. Syst. **16**, 746 (2007).

17) K. Sugano, K. Suekuni, T. Takeshita, K. Aiba, and Y. Isono, Jpn. J. Appl. Phys. **54**, 06FL03 (2015).

18) T. Takeshita, K. Suekuni, K. Aiba, K. Sugano, and Y. Isono, Electron. Commun. Jpn. **100**, 33 (2017).

19) K. Sugano, D. Matsui, T. Tsuchiya, and O. Tabata, Proc. Int. Conf. Micro Electro

255      Mechanical Systems, 2015, p. 608.

256 20)  S. Kumar, K. S. Gandhi, and R. Kumar, Ind. Eng. Chem. Res **46**, 3128 (2007).

257 21)  C. H. Munro, W. E. Smith, M. Garner, J. Clarkson, and P. C. White, Langmuir **11**, 3712

258      (1995).

259 22)  K. Sugano, Y. Uchida, O. Ichihashi, H. Yamada, T. Tsuchiya, and O. Tabata, Microfluid.

260      Nanofluid. **9**, 1165 (2010).

261 23)  M. Giersig and P. Mulvaney, Langmuir **9**, 3408 (1993).

262 24)  A. Dhawan, S. J. Norton, M. D. Gerhold, and T. Vo-Dinh, Opt. Express **17**, 9688 (2009).

263 25)  D. P. Fromm, A. Sundaramurthy, P. J. Schuck, G. Kino, and W. E. Moerner, Nano Lett. **4**,

264      957 (2004).

265 26)  K. Aiba, K. Ikegami, S. Yamazaki, K. Sugano, and Y. Isono, Denki Gakkai Ronbunshi E

266      **136**, 256 (2016) [in Japanese].

267 27)  L. Tang, H. Xu, and M. Käll, MRS Bull. **39**, 163 (2014).

268 28)  D. Radziuk, and H. Moehwald, Phys. Chem. Chem. Phys. **17**, 21072 (2015).

269 29)  L. A. Lane, X. Qian, S. Nie, Chem. Rev. **115**, 10489 (2015).

270 30)  Y. S. Yamamoto, M. Ishikawa, Y. Ozaki, T. Itoh, Front. Phys. **9**, 31 (2013).

271 31)  E. C. Le Ru, P. G. Etchegoin, MRS Bull. **38**, 631 (2013).

272 32)  H. Perry, A. Gopinath, D. L. Kaplan, L. Dal Negro, F. G. Omenetto, Adv. Mater. **20**, 3070

273      (2008).

274 33)  M. Suzuki, Y. Niidome, S. Yamada, Thin Solid Films **496**, 740 (2006).

275

276

## Figure Captions

**Fig. 1.** (Color online) Schematics of proposed and developed gold nanoparticle dimer arrays for SERS, which are fabricated by the nanotrench-guided self-assembly. After particle arrangement the adsorbed molecules cover the particle surfaces. The adsorbed molecules were removed before a Raman measurement for target molecules.

**Fig. 2.** (Color online) Experimental method for nanoparticle dimer arrangement by nanotrench-guided self-assembly.

**Fig. 3.** SEM images of gold nanoparticle dimer array: (a) $5 \times 5$ μm$^2$ region, and (b) enlarged view.

**Fig. 4.** (Color online) Raman spectra of adsorbed molecules depending on the polarization angle.

**Fig. 5.** (Color online) Mapping result of adsorbed molecules. The values in the figure show an integral value between 1500 and 1700 cm$^{-1}$.

**Fig. 6.** (Color online) Polarization angle dependences of the Raman intensity (experimental: adsorbed molecules) and Raman enhancement (analytical).

**Fig. 7.** (Color online) Raman spectra of acetone dicarboxylic acid used in the evaluation of the substrate enhancement. The letters indicate the sample numbers.

**Fig. 8.** (Color online) Raman spectra of 4,4'-bipyridine at $10^{-3}$ M (A, B, C) and $10^{-7}$ M (D, E, F). Red dotted lines indicate 4,4'-bipyridine-derived Raman peaks. The letters indicate the sample numbers.

**Fig. 9.** (Color online) Relationship between Raman intensities of adsorbed molecules and 4,4'-bipyridine at concentrations of $10^{-3}$ and $10^{-7}$ M. The letters indicate the sample numbers shown in Figs. 7 and 8.

308

309   **Fig. 10.** (Color online) Raman intensity variations of adsorbed and 4,4'-bipyridine molecules

310   after and before compensation at concentrations of $10^{-3}$ and $10^{-7}$ M.

311

312   **Table I.** Average, standard deviation, and CV of Raman intensities of adsorbed and 4,4'-

313   bipyridine molecules after and before compensation at concentrations of (a) $10^{-3}$ and (b)

314   $10^{-7}$ M.

315

(a)

| | Adsorbed molecule | 4,4'-bipyridine | After compensation |
|---|---|---|---|
| Average | 2185.3 | 302.2 | 279.3 |
| Standard deviation | 652.2 | 86.0 | 30.5 |
| CV [%] | 29.8 | 28.5 | 10.9 |

(b)

| | Adsorbed molecule | 4,4'-bipyridine | After compensation |
|---|---|---|---|
| Average | 1097.2 | 108.8 | 165.0 |
| Standard deviation | 731.1 | 49.3 | 18.8 |
| CV [%] | 66.6 | 45.3 | 11.4 |

316

317

318

Au nanoparticle dimer (φ=100nm)

Incident light (E)

Polarization: 0°

Reservoir

Chip size: 15×30mm

Si substrate

PDMS cover

Adsorbed molecules

Analyzed target molecules

Fig.1. (Color online)

colloidal aqueous solution

glass substrate

water surface line

DRYING

template substrate

assembled particles

meniscus
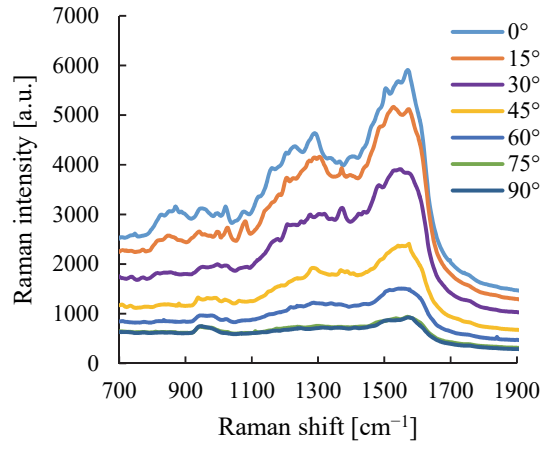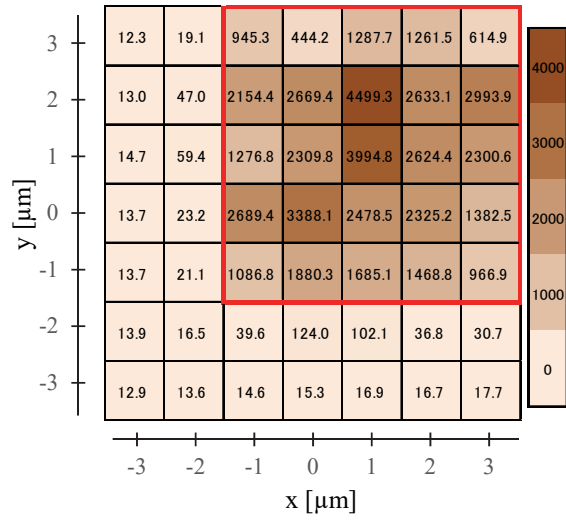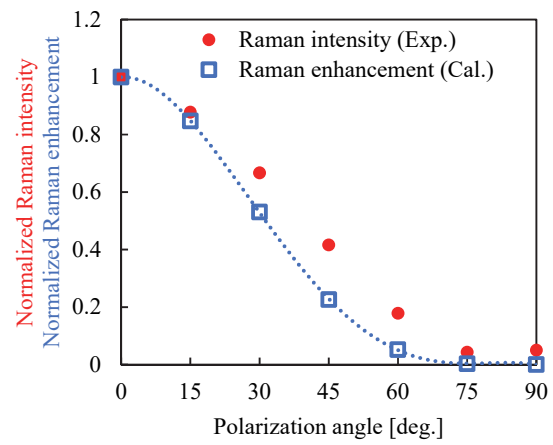
Fig.2. (Color online)

(a)

1 µm

(b)

200nm
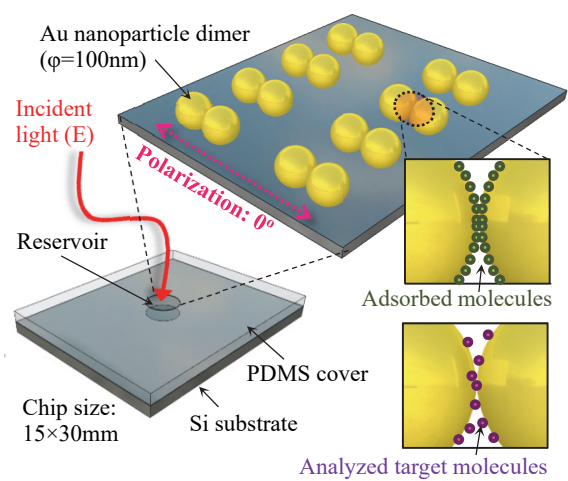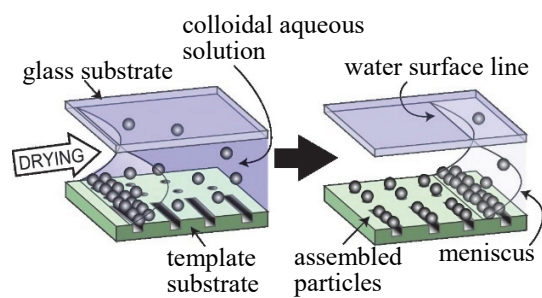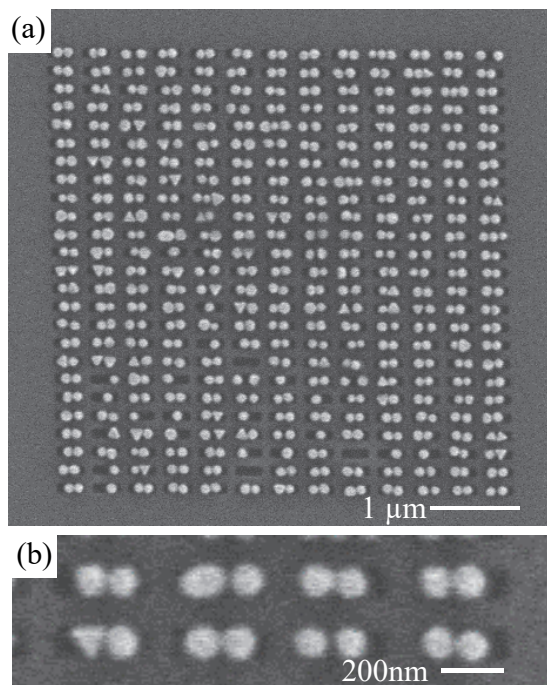
Fig.3.

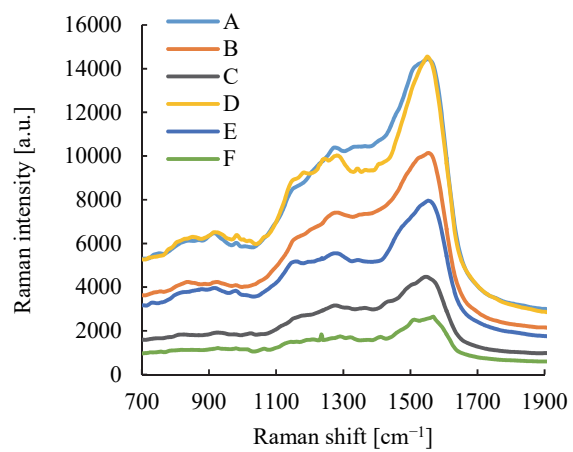Fig.4. (Color online)

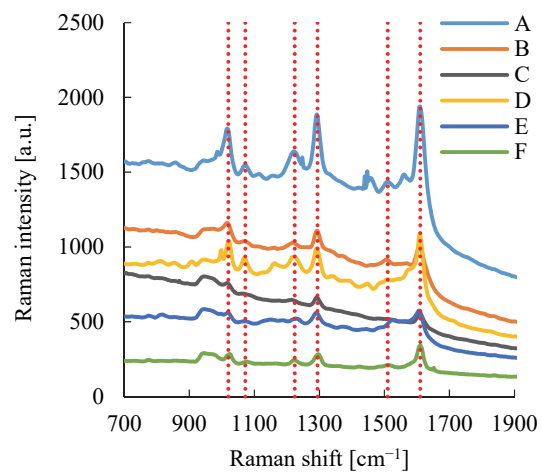Fig.5. (Color online)
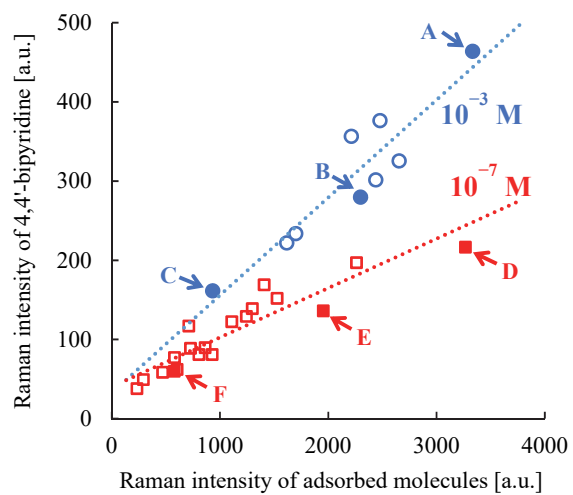
Fig.6. (Color online)

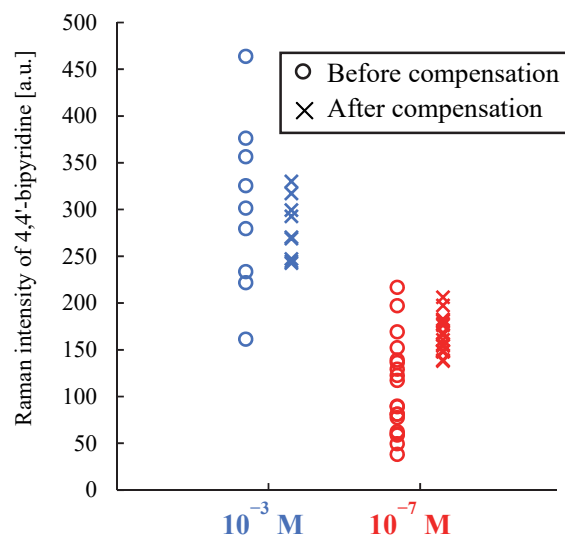Fig.7. (Color online)

Fig.8. (Color online)

Fig.9. (Color online)

Fig.10. (Color online)